Supporting Information

Experimental Section

Materials. L-Glutamate oxidase (GluOx) (G5921-5 UN), glucose oxidase (GOx) (G109029-10 kU), ascorbate oxidase (A0157-100 UN), 5 wt% Nafion solutions, L-glutamic acid (V900408), γ-aminobutyric acid (A5835), bovine serum albumin (BSA, V900933), K_2PtCl_6, 3-glycidoxypropyltrimethoxysilane (GOPS), dodecyl benzene sulfonic acid and 3,4-Dihydroxyphenylacetic acid (850217) were purchased from Sigma Aldrich Co. Phosphate-buffered saline (PBS) was acquired from Solarbio Science and Technology Co., Ltd. Poly(3,4-ethylene dioxythiophene):poly(styrene sulfonate) (PEDOT:PSS) aqueous dispersion (Clevios PH1000) was purchased from Heraeus. Ascorbic acid (A103534), uric acid (U105582), agarose (A104062) and glutaraldehyde (G105905) were purchased from Aladdin Reagent Database Inc. Glucose (P0028) was purchased from TCI. Dopamine hydrochloride was purchased from Damas-beta. Nylon fibers (0.05 mm) were purchased from Kuroda. Au wire (0.07mm) and Pt wire (0.07 mm) were purchased from Wuhu Ariter Mechanical and Electrical Equipment Co., Ltd. Dental adhesive resin cement was purchased by Nissin Dental Products Inc. All other common reagents were purchased from Sinopharm Chemical Reagent Co., Ltd.

Fabrication of CNT fibers. CNT fibers were synthesized by floating catalyst chemical vapor deposition using thiophene and ferrocene as catalysts, flowing argon (200 sccm) as carrier gas, and hydrogen (1600 sccm) as reducing gas at 1200 °C. The synthetic details are provided elsewhere.[S1]

Preparation of CNT/Platinum nanoparticles (Pt NPs) fibers. The CNT/Pt NPs fiber was prepared *via* an electrochemical double potential step method. The used solution included K_2PtCl_6 (1 mM) and KCl (0.1 M). Working, counter and reference electrodes were made of CNT fiber, Pt wire and Ag/AgCl, respectively. During an electrochemical cycle, the deposition was managed by setting the first step at 0.5 V for 10 s and the second step at -0.7 V for 10 s. The CNT/Pt NPs fibers were obtained by electroplating 0.02 C charge.

Preparation of CNT/Pt NPs/Nafion fibers. The CNT/Pt NPs/Nafion fiber was prepared by dip coating 2.5 μL 5 wt% Nafion onto the CNT/Pt NPs fiber for three times. For dopamine detection, the electrode was prepared by dip coating 2.5 μL 0.1 wt% Nafion onto the CNT/Pt NPs fiber for three times. The 0.1 wt% Nafion solution was made by diluting 5 wt% Nafion with ethanol.

Enzymes immobilization. GluOx was immobilized on the gate of OECT through crosslinking with glutaraldehyde, BSA, ascorbate oxidase and Nafion. The immobilization solution was prepared by mixing 20 μL solution of glutamate oxidase at 10 $UN \cdot mL^{-1}$, 10 μL solution of ascorbate oxidase at 1000 $UN \cdot mL^{-1}$, 1.5 mg BSA, 15 μL 0.01 M PBS, 2.5 μL 2.5 wt% glutaraldehyde solution and 2.5 μL of 5 wt% Nafion solution. 2.5 μL of the mixed solution was dip-coated onto the CNT/Pt NPs/Nafion fiber. CNT/Pt NPs/Nafion/GluOx fiber was then stored at 4 ℃ overnight before testing. For glucose detection, a similar solution was prepared *via* a mixture of GOx (glucose oxidase) instead of GluOx.

Fabrication of channel. Before sputtering, the nylon fiber was washed under ultrasonic treatment using acetone, alcohol and deionized water each for 30 minutes. Patterned Cr (5 nm)/Au (100 nm) drain and source electrodes were deposited onto a nylon fiber *via* thermal evaporation. Uniform coverage on fiber surface was ensured by hanging it on a sample holder during sputtering. The thickness of metal film was controlled *via* a thickness monitor of the deposition system. For the preparation of the PEDOT:PSS solution, 10 mL of PEDOT:PSS aqueous dispersion was added with 2.5 mL of ethylene glycol and 25 μL of dodecyl benzenesulfonic acid to improve the conductivity of PEDOT:PSS layer. And 1 wt% 3-glycidoxypropyltrimethoxysilane cross-linker was added into the dispersion to enhance the stability of PEDOT:PSS. Then the dip-coating method was conducted by immersing fiber into the resulting PEDOT:PSS solution and pulling it out at a constant speed for 36 times. The fiber with PEDOT:PSS layer was transferred to a glove box filled with N_2 for post-annealing at 140 ℃ for 1 hour and were immersed in deionized water to remove any excess low-molecular weight compounds. Then a parylene layer (~3 μm) was deposited onto the surface through a chemical vapor method as an encapsulation layer on the electrodes using specialty coating systems (SCS PDS2010 Labcoter®).

Characterization. The structures of the fiber-shaped devices were characterized using field emission scanning electron microscopy (Zeiss Ultra 55). Au nanoparticles were deposited at 10 mA for 60 s on the surface of the low-conductive materials. Nanoindentation tests for materials were performed using a Bruker Hysitron Ti-950 nanoindenter equipped with a standard Berkovich probe. 100 μN maximum normal force was applied with 0.02 mN/s loading rate, followed by 2-second holding and 5-second unloading segments in each test. Nano-indentation modulus was calculated from the unloading part in the load-displacement curve using Oliver-Pharr method. Nanoindentation tests for biological tissues were performed using a Piuma Nanoindenter (Optics 11 BV) equipped with a spherical indenter of 10 μm in diameter and 0.48 N/m in stiffness. Displacement control was operated by 2-second loading and 1-second holding. Nano-indentation modulus was calculated from the loading part in the load-displacement curve using Hertz model.

All electrical characterizations were done using 0.01 M PBS as electrolyte. Output and transfer characteristics were obtained using a Keithley K2410 with custom LabVIEW software and a CHI660e electrochemical workstation. The current versus time curves were recorded using a CHI660e electrochemical workstation with applied voltage of -0.6 V. The electrochemical stability was tested in A.C. impedance parameters. The three-electrode system was chosen with Ag/AgCl, Pt wire and bio-probe as reference, counter and working electrodes, respectively. They were immersed in 0.01 M PBS solution. The mechanical stability was tested after bending for total 2000 cycles with tensile testing machine. The electrochemical stability was tested under dynamic process to simulate the body movement with a frequency range of 0.01-10 Hz, which is accordance to breathy and heartbeat frequency. Anti-interference characterization was carried out in two ways. Firstly, different current responses were recorded at the same test, where the target substance and other interferences with the same concentration were added to the stirring electrolyte. The second one is that the target substance and other interferences were gradually added to the stirring electrolyte from low to high concentrations with the same device at the respective tests. Therefore, the individual current response was achieved as a function of the concentration. Accordingly, the slope is calculated as sensitivity.

All animal experiment protocols were approved by Animal Experimentation Committee of Fudan University. All animals were treated according to guidelines for

the care and use of experimental animals described by the National Institutes of Health and Fudan University. Male mice (BALB/c, 5 weeks old) were purchased from Shanghai Jiesijie experimental animal Co., Ltd and kept with controlled humidity and temperature. Mice were sacrificed after fiber-shaped OECTs were implanted for 7 days. Brains removed from the mice were fixed with 4% (v/v) paraformaldehyde in 0.01 M PBS solution. For immunofluorescence staining, antigen retrieval was performed by heating in 0.01 M citrate buffer (pH 6.0). NeuN (1:50, GB13138, Servicebio) and GFAP (1:500, GB11096, Servicebio) was used as primary antibody and 488 conjugated goat anti-mouse (1:400, GB25301, Servicebio) and Cy3 conjugated goat anti-rabbit IgG (H+L) (1:300, GB21303, Servicebio) were used as secondary antibody. Immunofluorescence sections were mounted with DAPI Fluoromount-G® (0100-20, Southern Biotech) and observed under fluorescent microscopy (Olympus BX51).

In vivo detection of glutamate and electrophysiology record. The mouse was anesthetized with 2% isoflurane. After implantation of glutamate-OECT in hippocampus of mouse brain, real-time monitoring of glutamate was performed by tail intravenous injection of picrotoxin solution (1.0 mg/mL, 0.3 mL) and 0.9% NaCl solution (0.3 mL) *via* 1 mL syringe. All the conditions were controlled the same except for the picrotoxin solution and 0.9% NaCl solution between the experimental and control groups. The local field potential was recorded simultaneously *via* the recording electrode implanted in the opposite hippocampus and the reference electrode implanted in the skull near epencephalon using electrophysiological recording instrument (Blackrock cereplex direct). The recording and reference electrodes were made of copper wire which had conducting tips with polymer insulation around the wires. The local field potential data was processed with NeuroExplorer software.

In vivo detection of dopamine. The mouse was anesthetized with 2% isoflurane. After implantation of dopamine-OECT in hippocampus of mouse brain, real-time monitoring of dopamine was performed by intracerebral microperfusion of dopamine solution (5 mM, 3 μL) and 0.9% NaCl solution (3 μL) at 0.3 μL per minute using quintessential stereotaxic injector (Stoelting Co. 53311). The site of injection was next to the fiber-shaped OECT about 2 mm distance. All the conditions were controlled the same except for the dopamine solution and 0.9% NaCl solution

between the experimental and control groups. For *in vivo* anti-interference characterization, dopamine, ascorbic acid and uric acid were injected into the brain with 1 μL of the same 5 mM concentration at a constant flow rate of 0.2 μL/min. During 7 days of detection of dopamine, the dopamine-OECT was fixed on the mouse head with dental cement.

Table S1. Effective Young's moduli of mice tissues measured by nanoindentation.

Biological tissue	Young's modulus/kPa
Brain	0.41 ± 0.11
Heart	3.05 ± 0.80
Liver	5.97 ±2.92
Lung	0.40 ± 0.14
Muscle	8.10 ± 8.49
Spleen	33.26 ± 16.45
Kidney	11.57 ± 1.55
Skin	51.83 ± 21.82
Stomach	16.21 ± 5.36

Table S2. Reported elastic moduli of common materials.

Materials	Type	Geometry and size	Transverse modulus (GPa)	Longitudinal modulus (GPa)	Ref.
carbon fiber	M 40	fiber, diameter: 5.8 μm	15 ± 4.9	294	[S2]
	M 46	fiber, diameter: 5.6 μm	14 ± 5.7	377	
Au	/	wire, diameter: 10-1000 μm	74.08 ± 1.44	/	[S1]
silicon	/	shank, width: 20-144μm thickness: 14.75-100 μm	134 ± 1.31	/	[S1]
parylene	/	film	2.69 ± 0.03	/	[S3]
polyimide	/	/	3.526 - 6.84	/	[S4–S6]
nylon 66	/	/	2.27 ± 0.21	/	[S7]
nylon 11	/	/	1.351 ± 0.034	/	[S8]
nylon 6	γ-form	/	1.18 ± 0.02	/	[S9]
	(α + γ)-form	/	1.75 ± 0.36	/	
	α-form	/	2.5 ± 0.08	/	
silicon (100)	/	/	165 - 172	/	[S10–S12]

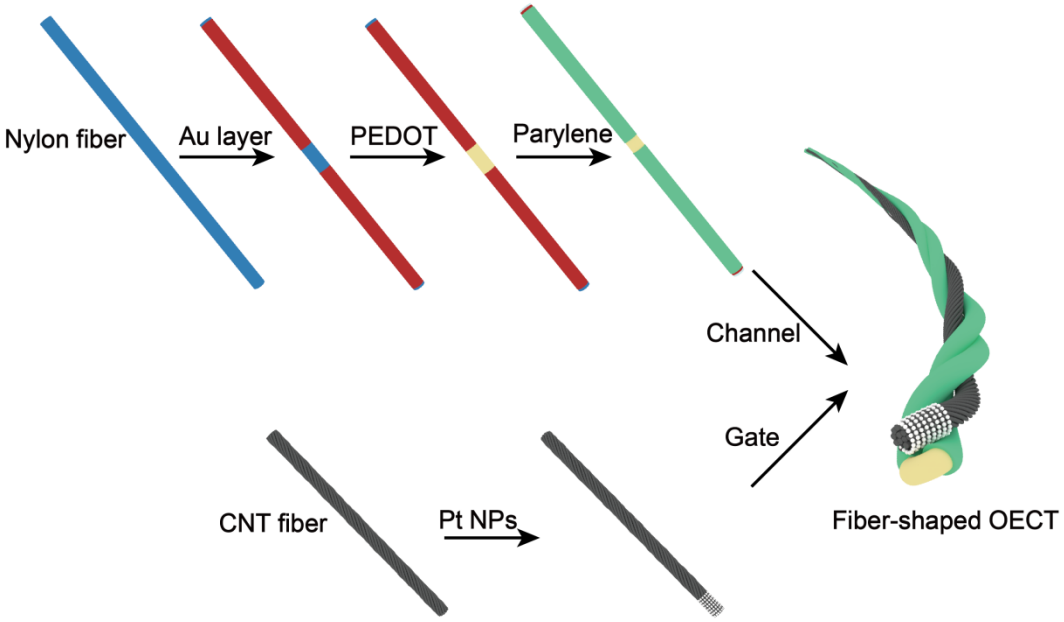

Figure S1. The fabrication process of channel and gate electrode of the fiber-shaped all-in-one OECT.

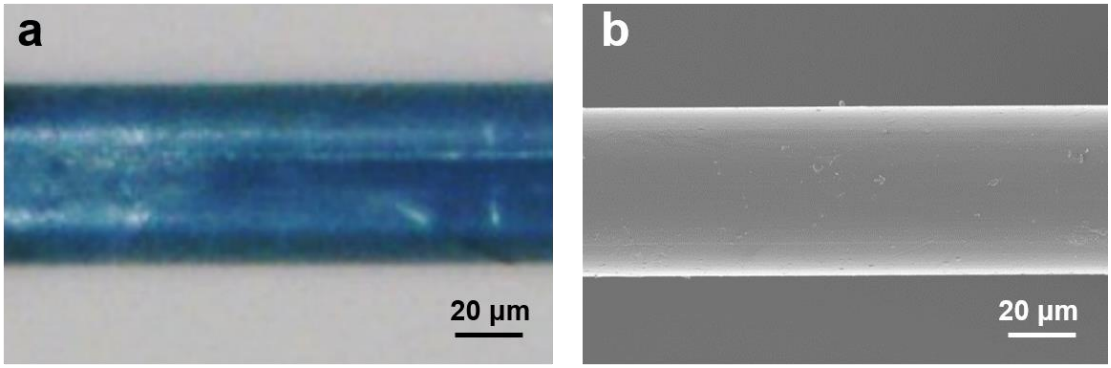

Figure S2. (**a** and **b**) Photograph and SEM image of semiconductor PEDOT:PSS coated on the nylon fiber between source and drain electrodes.

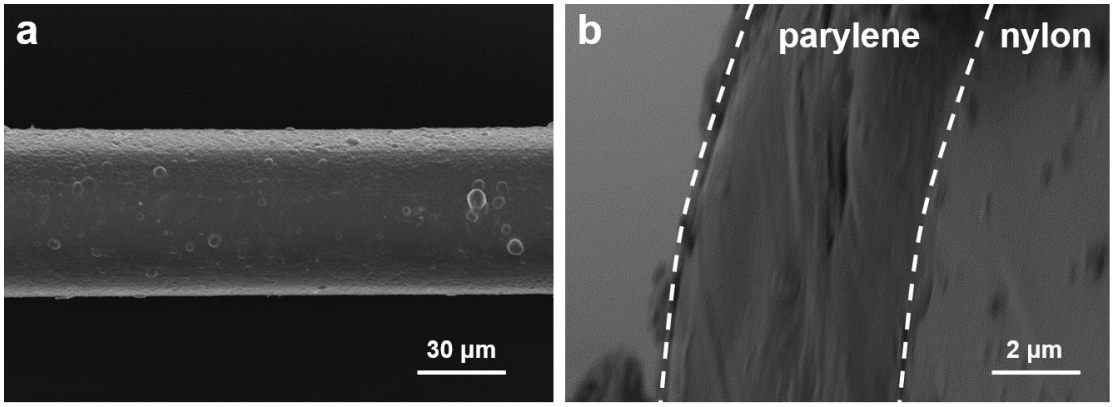

Figure S3. (**a** and **b**) Side and cross-sectional SEM images of the parylene insulated layer outside the nylon fiber.

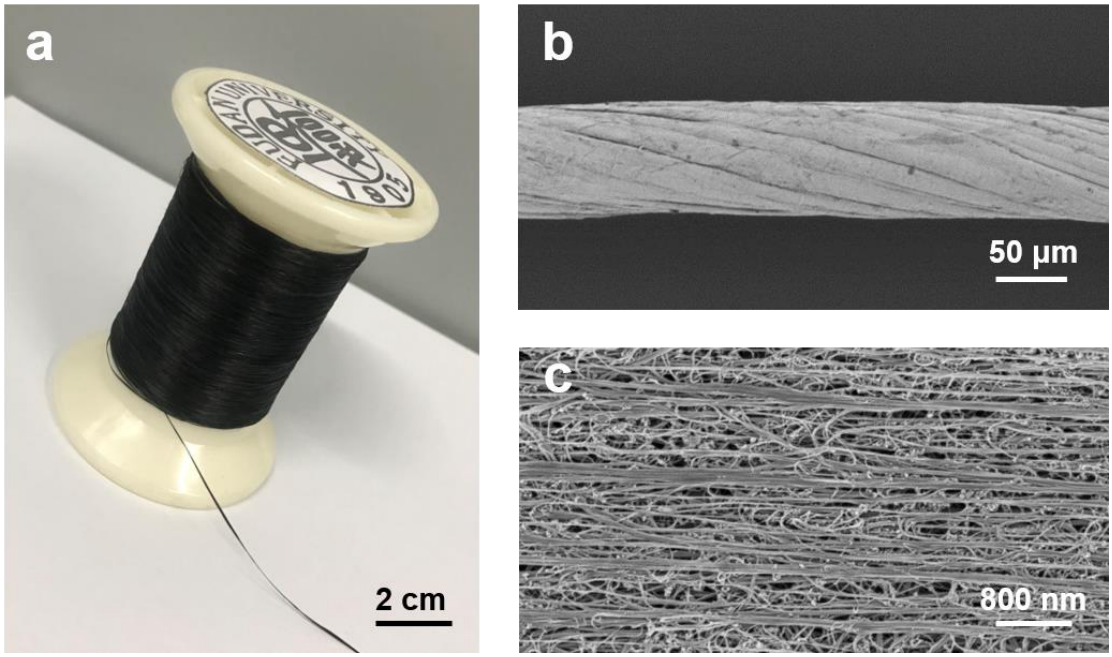

Figure S4. (**a**) Optical image of a roll of CNT fiber. (**b** and **c**) SEM images of a CNT fiber at low and high magnifications, respectively.

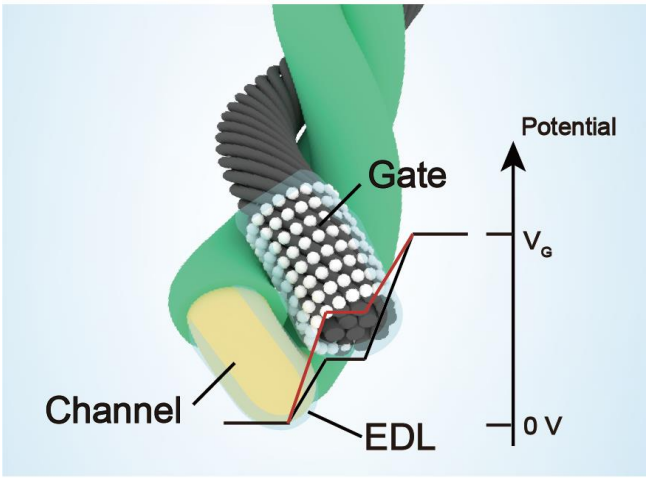

Figure S5. The working mechanism of the fiber-shaped all-in-one OECT.

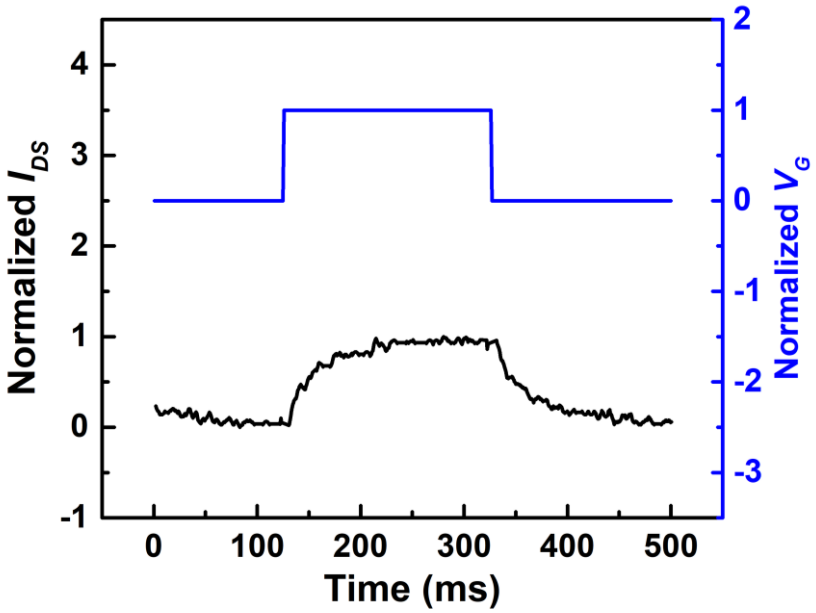

Figure S6. Normalized drain current changes as a consequence to normalized pulse voltage applied to the gate.

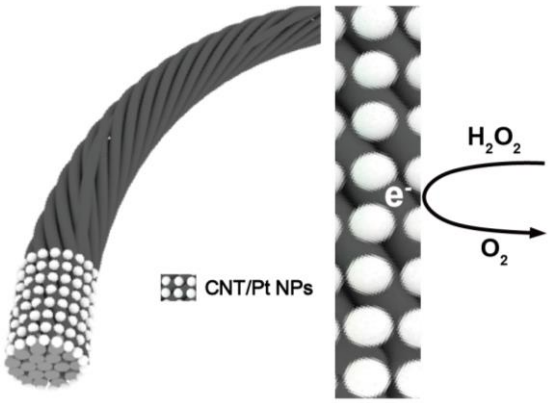

Figure S7. Schematic illustration for the gate electrode of fiber-shaped H_2O_2-OECT and the mechanism of H_2O_2 detection.

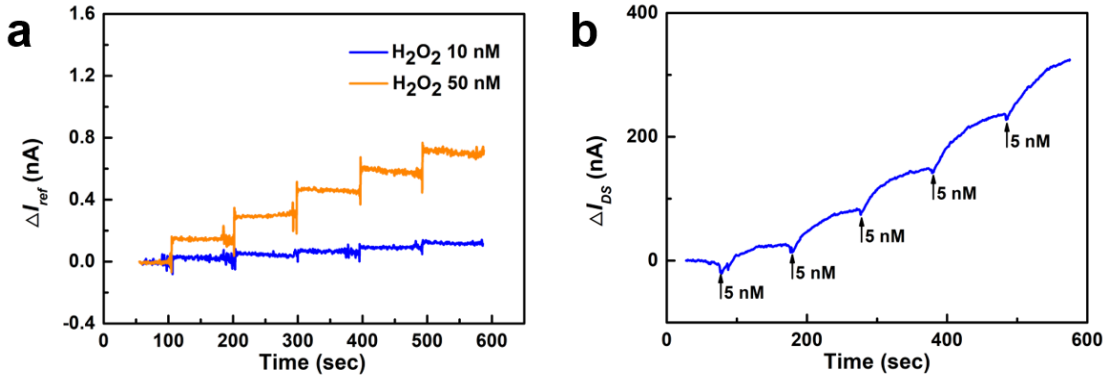

Figure S8. (**a**) Current versus time with the addition of H_2O_2 as potential of 0.4 V vs Ag/AgCl for the CNT fiber. (**b**) Drain current of the OECT in response to addition of H_2O_2. V_D and V_G were fixed at -0.6 V and 0.4 V, respectively.

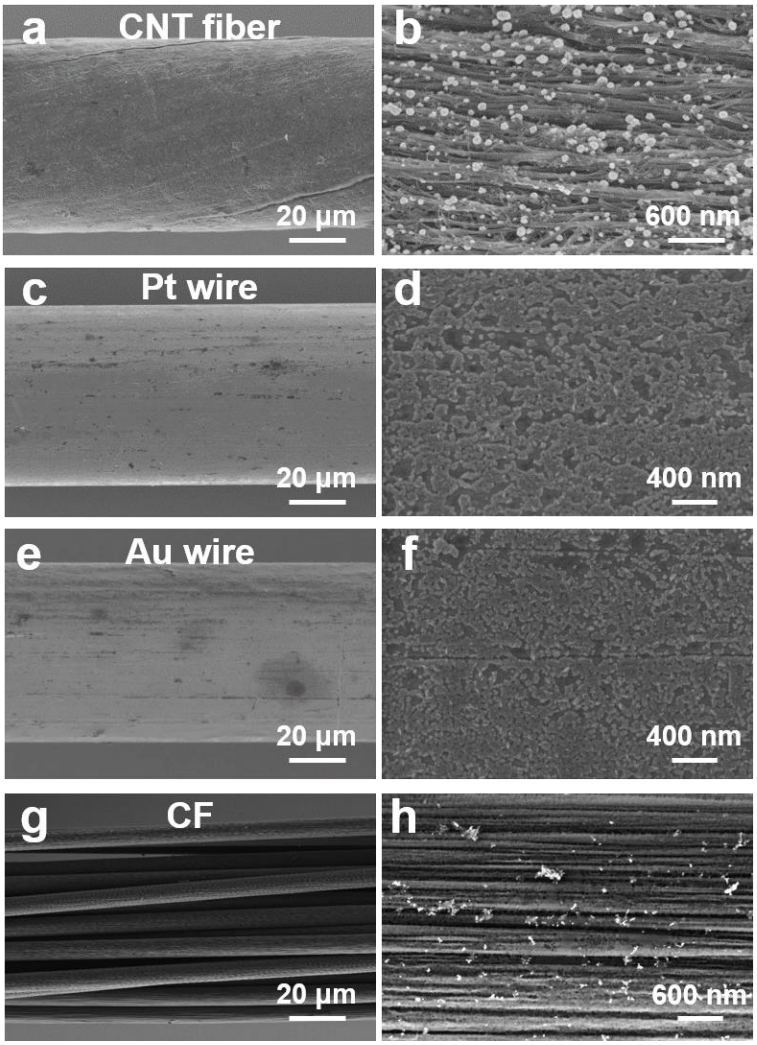

Figure S9. SEM images of CNT fiber (**a-b**), Pt wire (**c-d**), Au wire (**e-f**) and carbon fiber (CF, **g-h**) deposited with Pt NPs at low (**a, c, e, g**) and high (**b, d, f, h**) magnifications.

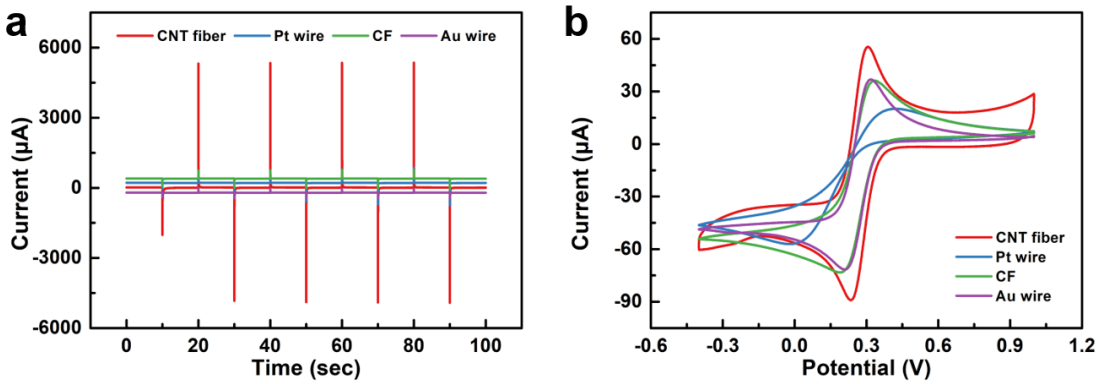

Figure S10. (**a**) Amperometric curves of different fiber electrodes during the platinum electrodeposition process. (**b**) Cyclic voltammograms of CNT fiber, Pt wire, CF and Au wire determined in the potassium ferricyanide solution.

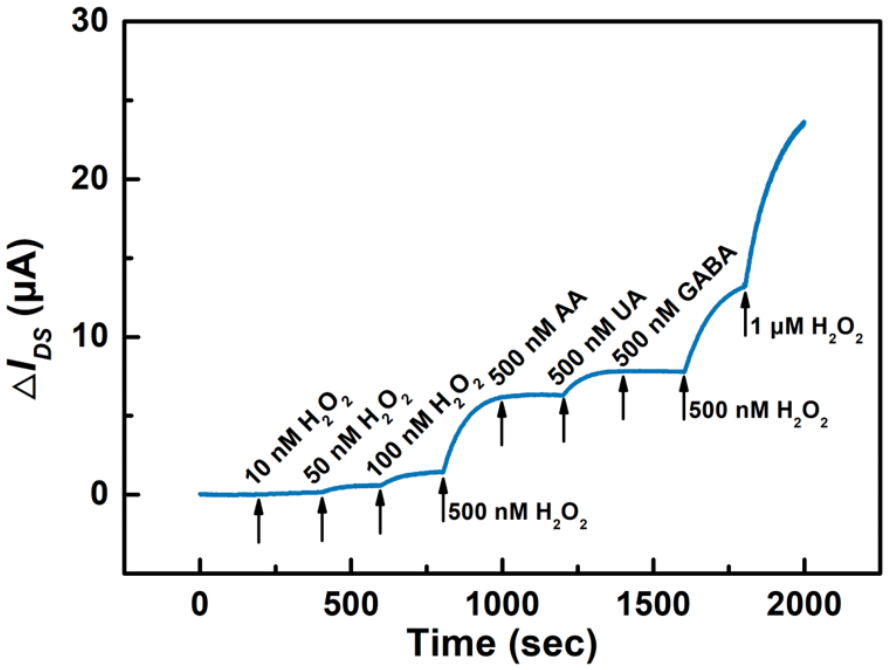

Figure S11. The anti-interference characterization of the H_2O_2-OECT.

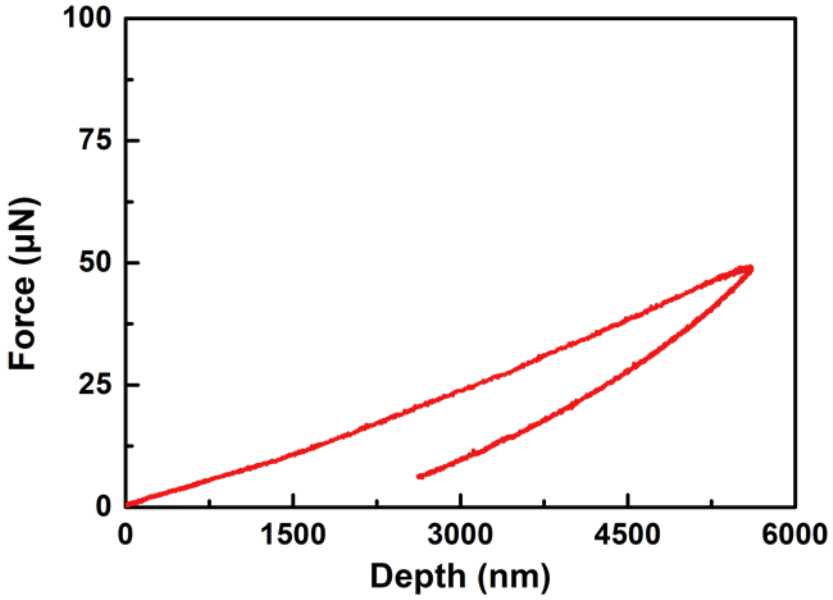

Figure S12. Indentation force versus indentation depth of CNT fiber.

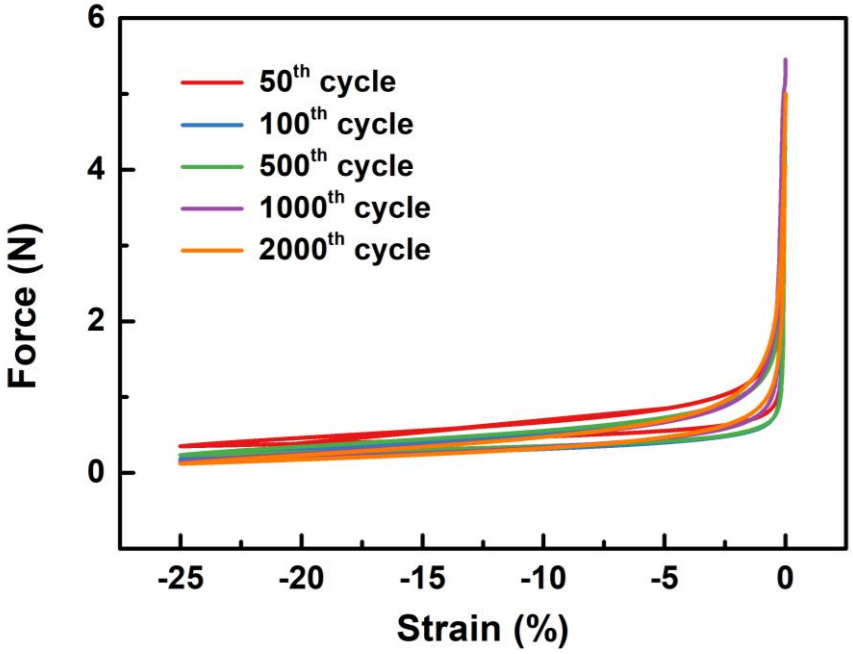

Figure S13. Force-strain curves of fiber-shaped OECTs under different bending cycles.

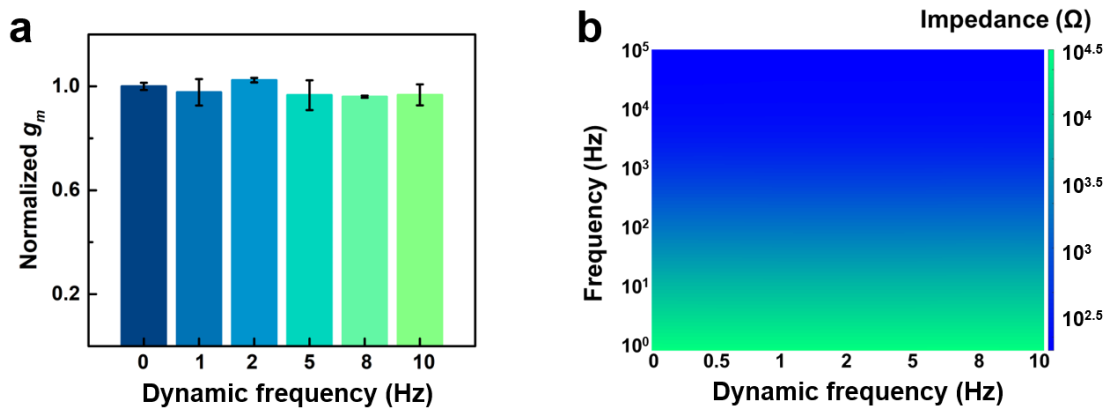

Figure S14. (**a** and **b**) Normalized transconductance of channel and impedance of gate electrode under different dynamic frequencies, respectively.

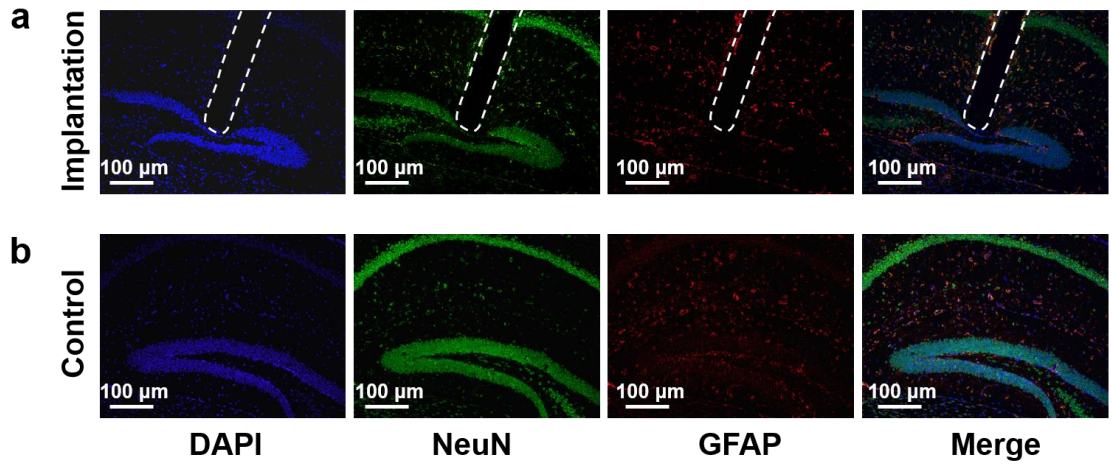

Figure S15. Representative fluorescence images of coronal brain slices showing (**a**) the wound created by implanted fiber-shaped OECT for 7 days and (**b**) control group without implants. Immunofluorescent staining for 4',6-diamidino-2-phenylindole (DAPI, blue), neurons (NeuN, green), glial fibrillary acidic protein (GFAP, red) and the merged signals are provided for clarification. The white dotted line indicates the position of fiber-shaped device.

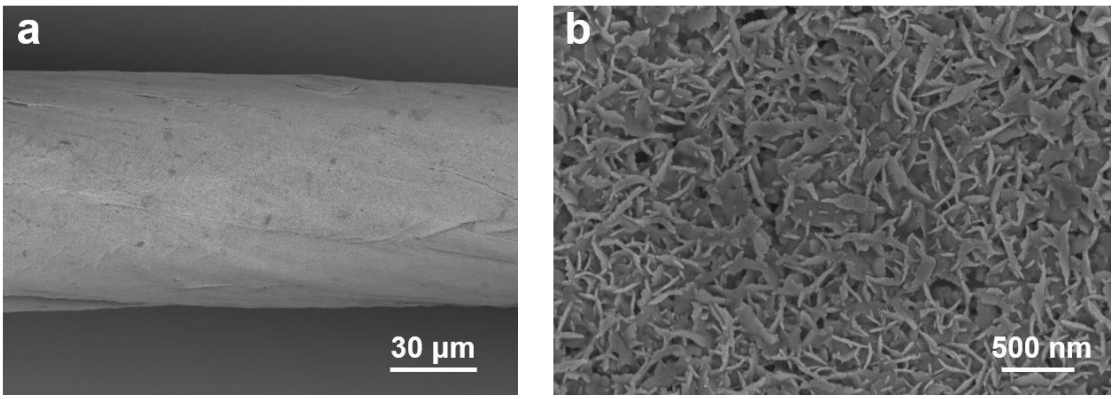

Figure S16. (**a** and **b**) SEM images of a CNT/Pt NPs/Nafion fiber at low and high magnifications, respectively.

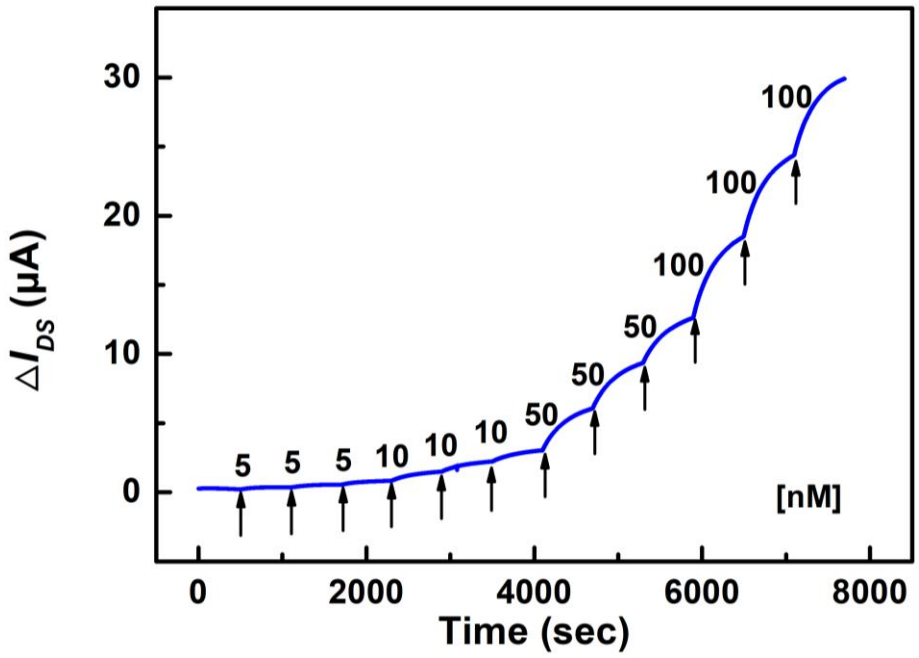

Figure S17. Drain current responses of a fiber-shaped OECT to the addition of DA with different concentrations.

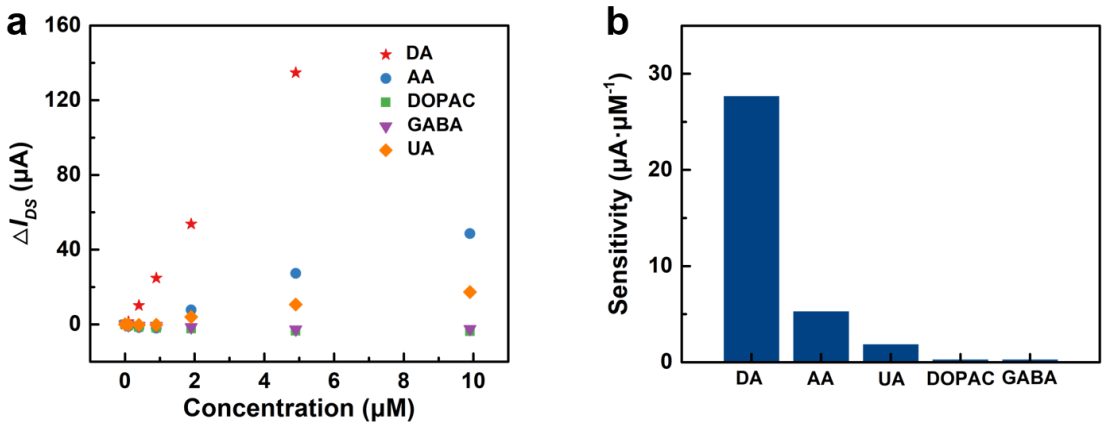

Figure S18. (**a**) The corresponding drain current changes of dopamine-OECT to the additions of DA and four major interferences (including AA, UA, DOPAC and GABA) with different concentrations. (**b**) The sensitivity characterization of these five biochemicals with the same dopamine-OECT (sensitivities were calculated by the slope of **a**).

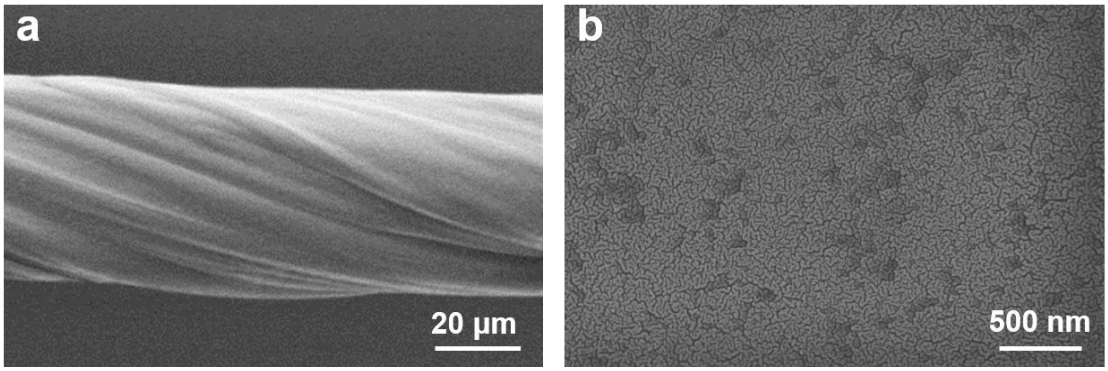

Figure S19. (**a** and **b**) SEM images of a CNT/Pt NPs/Nafion/GluOx fiber at low and high magnifications, respectively.

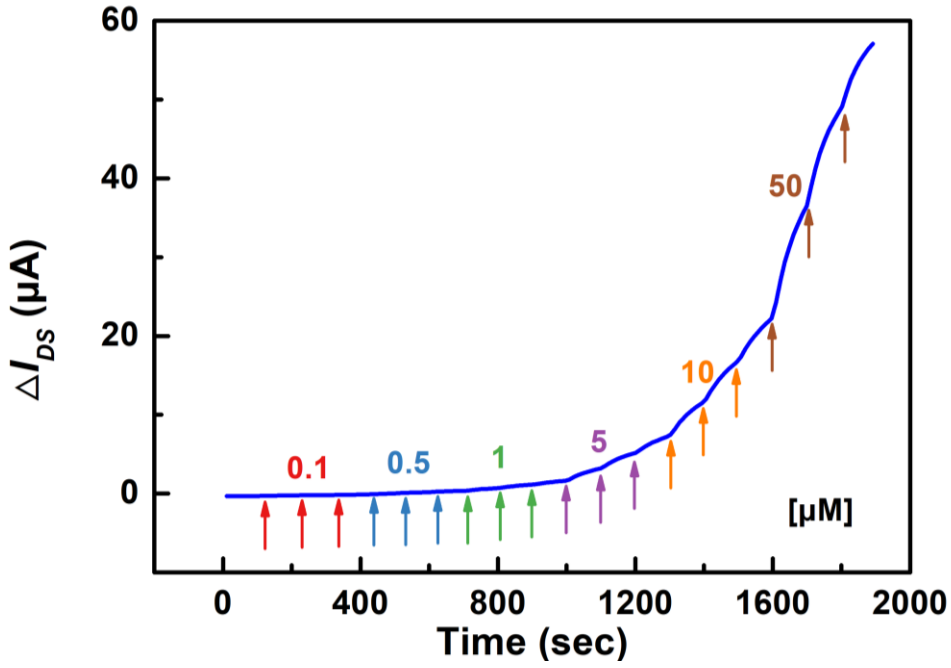

Figure S20. Drain current responses of a fiber-shaped OECT to the addition of glutamate with different concentrations.

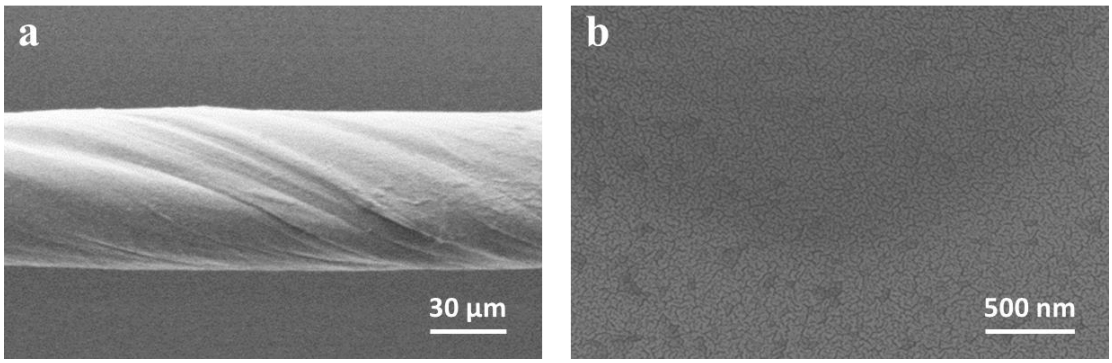

Figure S21. (**a** and **b**) SEM images of a CNT/Pt NPs/Nafion/GOx fiber at low and high magnifications, respectively.

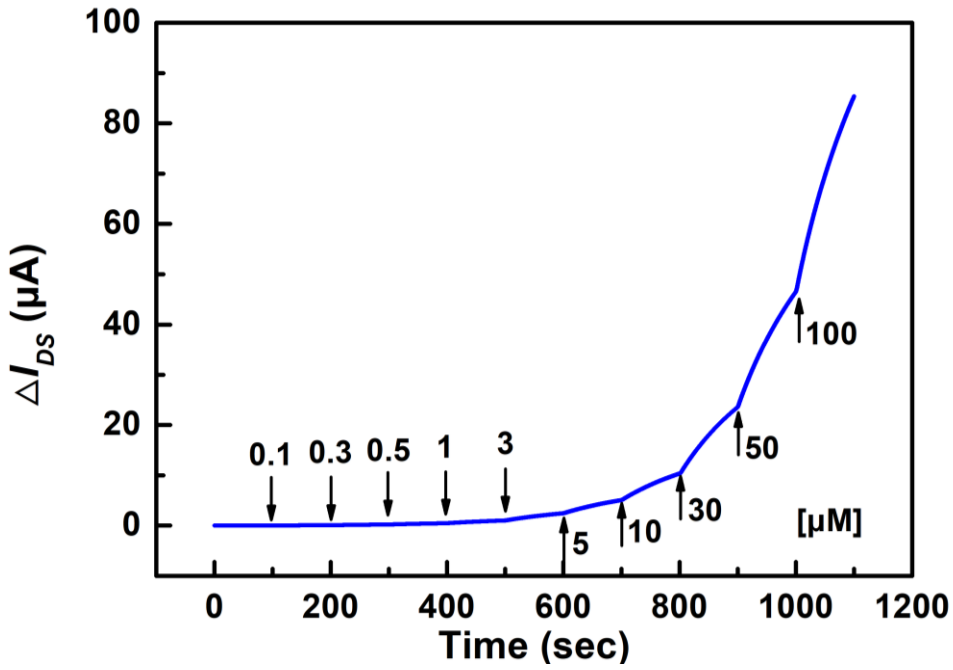

Figure S22. Drain current responses of a fiber-shaped OECT to the addition of glucose with different concentrations.

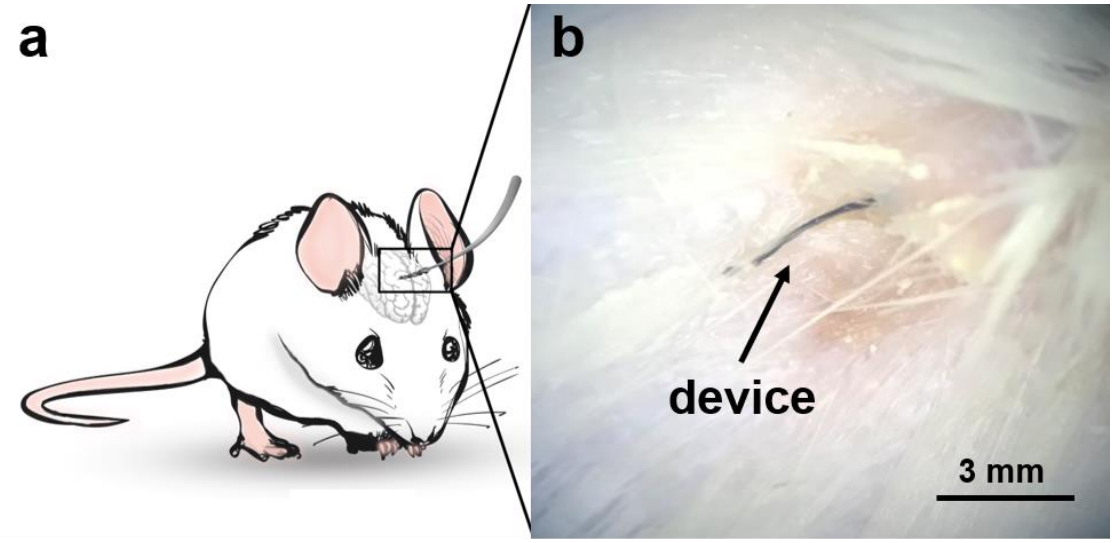

Figure S23. (**a**) The schematic diagram of the mouse implanted with the fiber-shaped OECT. (**b**) Photograph of the mouse implanted with the fiber-shaped OECT.

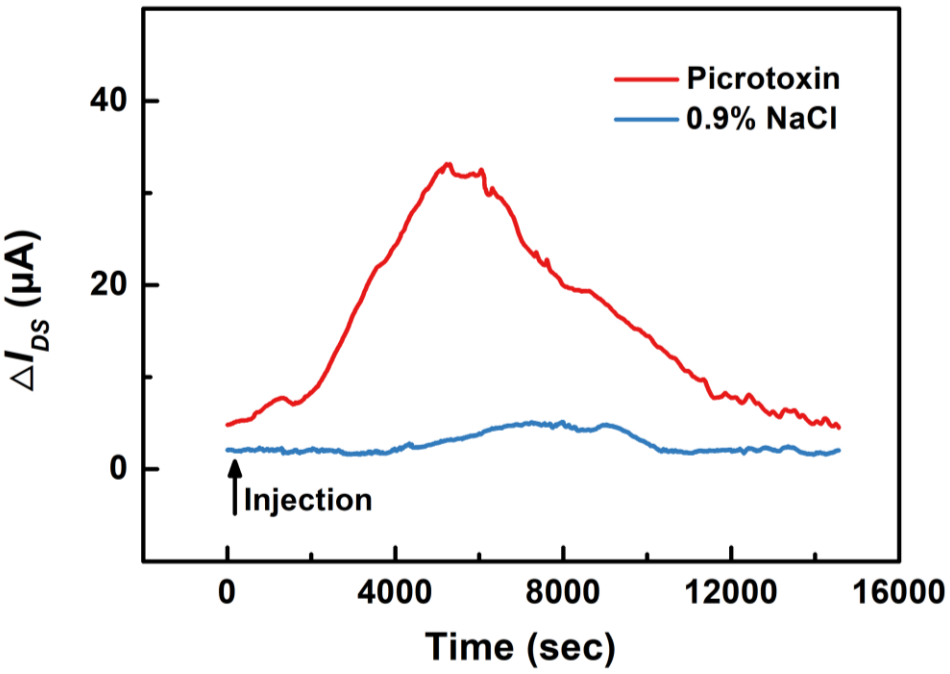

Figure S24. Real-time monitoring of the current responses of the glutamate-OECT in mouse brain under epilepsy induced by intravenous injection of 0.3 mL 1 mg/mL picrotoxin solution (red line) and control group using 0.9% NaCl solution (blue line).

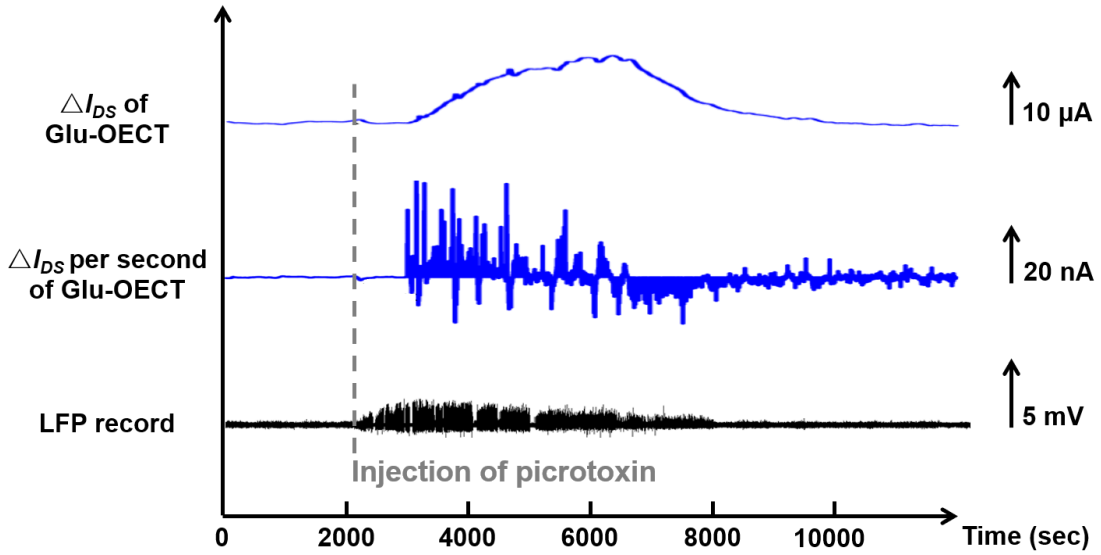

Figure S25. Real-time monitoring of the current response using the glutamate-OECT (blue line) and local field potential (LFP, black line) in mouse brain under epilepsy induced by intravenous injection of 0.3 mL 1 mg/mL picrotoxin solution. The gray dotted line indicates the timing of injection of picrotoxin solution.

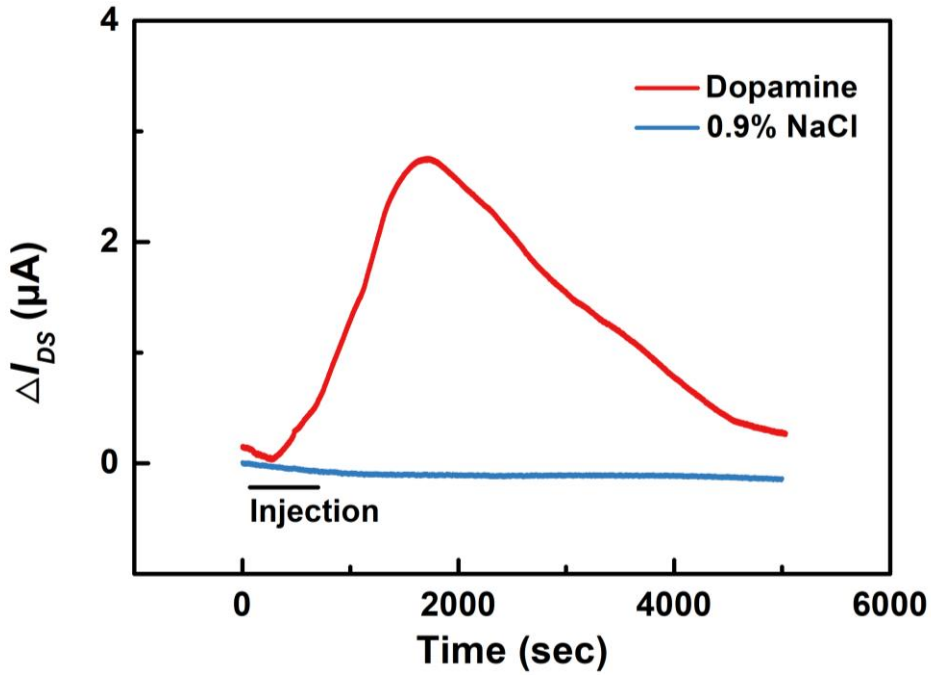

Figure S26. Real-time monitoring of the current response using dopamine-OECT in mouse brain by intracerebral microperfusion of 3 μL 5 mM DA solution at a constant flow rate of 0.3 μL/min (red line) and control group using 0.9% NaCl solution (blue line).

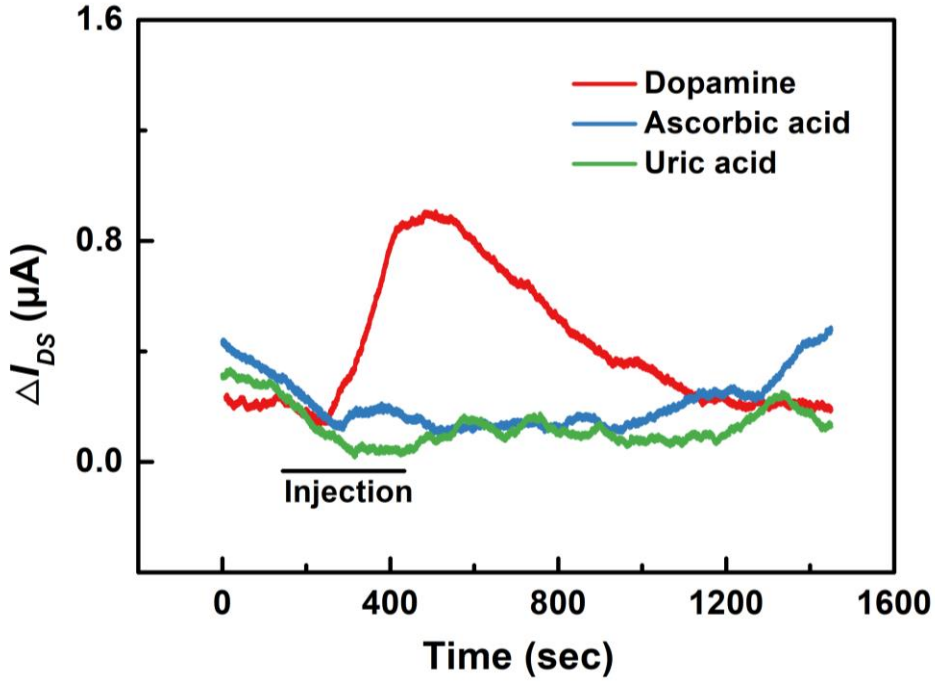

Figure S27. *In vivo* anti-interference characterization of the dopamine-OECT in the same mouse brain by intracerebral microperfusion of 1 μL 5 mM DA solution (red line), AA (blue line) and UA (green line) at a constant flow rate of 0.2 μL/min.

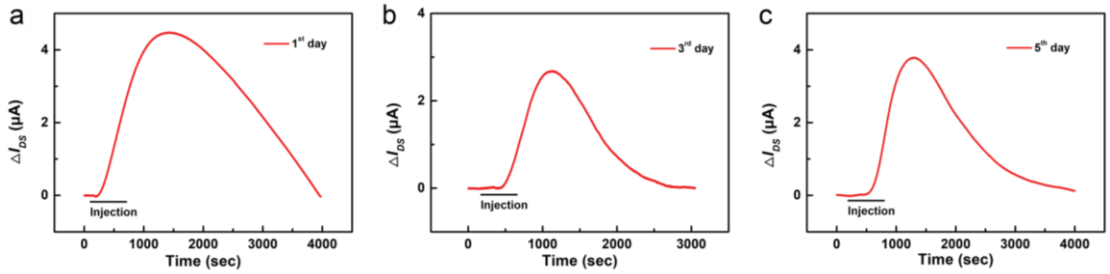

Figure S28. (**a-c**) *In vivo* detection of DA using the dopamine-OECT for one, three and five days in the same mouse brain, respectively. The experiments were performed by intracerebral microperfusion of 3 μL 5 mM DA solution at a constant flow rate of 0.3 μL/min.

References for the Supporting Information

S1 Wang L, Xie S, Wang Z, Liu F, Yang Y, Tang C, Wu X, Liu P, Li Y, Saiyin H, Zheng S, Sun X, Xu F, Yu H, Peng H. *Nat Biomed Eng*, 2020, 4: 159–171

S2 Maurin R, Davies P, Baral N, Baley C. *Appl Compos Mater*, 2008, 15: 61–73

S3 Kim BJ, Chen B, Gupta M, Meng E. *J Micromechanics Microengineering*, 2014, 24: 065003

S4 Lu YC, Jones DC, Tandon GP, Putthanarat S, Schoeppner GA. *Exp Mech*, 2010, 50: 491–499

S5 Beake BD, Smith JF. *Philos Mag A*, 2002, 82: 2179–2186

S6 Lee C, Kwon J, Park S, Sundar S, Min B, Han H. *J Polym Sci Part B Polym Phys*, 2004, 42: 861–870

S7 Shen L, Phang IY, Chen L, Liu T, Zeng K. *Polymer*, 2004, 45: 3341–3349

S8 Hu Y, Shen L, Yang H, Wang M, Liu T, Liang T, Zhang J. *Polym Test*, 2006, 25: 492–497

S9 Shen L, Phang IY, Liu T. *Polym Test,* 2006, 25: 249–253

S10 Qian L, Li M, Zhou Z, Yang H, Shi X. *Surf Coatings Technol*, 2005, 195: 264–271

S11 Li X, Bhushan B, Takashima K, Baek CW, Kim YK. *Ultramicroscopy*, 2003, 97: 481–494

S12 Fang TH, Chang WJ, Lin CM. *Microelectron Eng*, 2005, 77: 389–398